Transportation Research Part D 46 (2016) 40–55

Contents lists available at ScienceDirect

Transportation Research Part D

journal homepage: www.elsevier.com/locate/trd

Can we reliably assess climate mitigation options for air traffic scenarios despite large uncertainties in atmospheric processes?

K. Dahlmann [a,*], V. Grewe [a,b], C. Frömming [a], U. Burkhardt [a]

[a] Deutsches Zentrum für Luft- und Raumfahrt, Institut für Physik der Atmosphäre, Oberpfaffenhofen, Germany
[b] Delft University of Technology, Faculty of Aerospace Engineering, Section Aircraft Noise & Climate Effects, Netherlands

ARTICLE INFO

Article history:
Available online 29 March 2016

Keywords:
Uncertainties
Climate impact
Aviation
Monte Carlo simulation

ABSTRACT

Air traffic has an increasing influence on climate; therefore identifying mitigation options to reduce the climate impact of aviation becomes more and more important. Aviation influences climate through several climate agents, which show different dependencies on the magnitude and location of emission and the spatial and temporal impacts. Even counteracting effects can occur. Therefore, it is important to analyse all effects with high accuracy to identify mitigation potentials. However, the uncertainties in calculating the climate impact of aviation are partly large (up to a factor of about 2). In this study, we present a methodology, based on a Monte Carlo simulation of an updated non-linear climate-chemistry response model AirClim, to integrate above mentioned uncertainties in the climate assessment of mitigation options. Since mitigation options often represent small changes in emissions, we concentrate on a more generalised approach and use exemplarily different normalised global air traffic inventories to test the methodology. These inventories are identical in total emissions but differ in the spatial emission distribution. We show that using the Monte Carlo simulation and analysing relative differences between scenarios lead to a reliable assessment of mitigation potentials. In a use case we show that the presented methodology can be used to analyse even small differences between scenarios with mean flight altitude variations.

1. Introduction

Climate change and its consequences are more and more of public concern, especially since the last report of the Intergovernmental Panel on Climate Change (IPCC, 2013). It is extremely likely that more than half of the observed increase in global average surface temperature from 1951 to 2010 was caused by the anthropogenic increase in greenhouse gas concentrations and other anthropogenic forcings (IPCC, 2013).

The climate impact of current air traffic contributes 4.9% with a range of 2–14% to global warming in terms of radiative forcing (Lee et al., 2009) and air traffic is expected to grow further by about 5% per year (ICAO, 2013). Thus, it is more and more important to reduce the climate impact of aviation. For mitigation measures, it is not sufficient to analyse CO_2 emissions only, as non-CO_2 effects play a crucial role (IPCC, 1999; Lee et al., 2009). The most important non-CO_2 effects are water vapour emission (IPCC, 1999), formation of line-shaped contrails (Schumann, 1996) and contrail cirrus (Burkhardt and Kärcher, 2011), as well as NO_x emissions ($NO_x = NO + NO_2$) which lead to changes in ozone and methane concentrations

* Corresponding author.
E-mail address: Katrin.Dahlmann@dlr.de (K. Dahlmann).

http://dx.doi.org/10.1016/j.trd.2016.03.006
1361-9209/

(e.g. Grooß et al., 1998). These non-CO_2 effects are particularly important for the climate impact of air traffic as their impact depends on the location of the emission. This refers to contrail formation and chemistry effects, such as the formation of ozone (Schumann, 2000; Grewe et al., 2002a; Grewe and Stenke, 2008; Rädel and Shine, 2008; Köhler et al., 2008; Frömming et al., 2012; Köhler et al., 2013; Williams et al., 2014), and the radiative response to a local perturbation (Lacis et al., 1990; Stuber et al., 2005). Dahlmann et al. (2011), for example, show that the ozone production efficiency of air traffic NO_x emissions is twice as large as that of surface emissions, e.g. by road traffic. In addition, the climate impact from air traffic-induced ozone change is larger than that of an ozone change at the Earth's surface, because the radiative impact of a greenhouse gas increases with increasing temperature difference between the surface and the atmospheric layer into which it is emitted (Lacis et al., 1990). The formation of contrails also depends strongly on the location of the emission, since persistent contrails only form in ice supersaturated regions, which occur mainly near the tropopause (Sausen et al., 1998). The impact of contrails depends on the altitude and latitude of the emission location, as the altitude of the tropopause and the available water for deposition depends on the latitude (Newinger and Burkhardt, 2012). Due to the dependency of the climate impact on altitude and latitude of different emissions, there is no general linear relationship between fuel consumption and climate impact. Therefore, mitigation options can lead to counteracting effects. On the one hand, a general reduction in flight altitude, for example, leads to a reduced climate impact from ozone, water vapour, and contrail formation (Frömming et al., 2012). On the other hand, a reduction in flight altitude leads to increased fuel consumption and thus to an increased climate impact from CO_2 (Frömming et al., 2012). Hence, it is important to simultaneously include all relevant climate agents when assessing the climate impact of mitigation scenarios.

The analysis of the climate impact of aviation, from the emission to changes in atmospheric concentrations, changes in radiation and temperatures, and consequently the decision which mitigation option has the highest reduction potential is complicated because of large uncertainties in the calculation of the atmospheric changes due to aviation emissions (Lee et al., 2009). A large part of the uncertainties arises from a spread of model results due to different calculation methods (e.g. different chemistry or cloud schemes). To ensure a reliable assessment of mitigation options, it is necessary to base it on statistically significant results, and therefore it is important to include uncertainty considerations.

The objective of this paper is to introduce a methodology that enables a reliable assessment of mitigation potentials for different emission scenarios despite large uncertainties in the overall climate impact of aviation. We introduce the methodology and present the principle mechanism with an example, which shows that although considerable uncertainties in the overall climate impact from air traffic exist, a reliable assessment of mitigation options can be achieved. Finally, a use case is presented, which assesses general flight altitude changes.

2. Method

2.1. AirClim – an efficient assessment tool

The climate impact of air traffic emissions is usually calculated in detail by using a complex three dimensional climate chemistry model, which considers all relevant atmospheric processes (e.g. Grewe et al., 2002b; Köhler et al., 2008; Hoor et al., 2009). As these simulations are computationally very expensive, it is not possible to use them for uncertainty assessments within Monte Carlo simulations, where the uncertainty is analysed by a large number of random experiments. Instead, we use the climate response model AirClim (Grewe and Stenke, 2008) in this study. AirClim combines precalculated atmospheric impact data with air traffic emission data to calculate e.g. aviation climate impact for a multitude of emission inventories. For the precalculated data, idealised emission regions with normalised emission strength are defined. For each of the idealised emission regions, a climate-chemistry simulation is performed, employing normalised emissions of nitrogen oxides and water vapour to obtain the chemical response, i.e. the simultaneous effect of nitrogen oxides and water vapour. Chemical perturbations and radiative forcing of ozone (O_3), methane (CH_4), water vapour (H_2O), and contrails are calculated with a state-of-the-art climate-chemistry model (E39/CA, e.g. Stenke et al. (2008)). For contrail cirrus we have used ECHAM4-CCMod (Burkhardt and Kärcher, 2009). The results of these detailed simulations constitute the precalculated atmospheric input data for AirClim. AirClim combines the precalculated, altitude and latitude dependent perturbations with emission data in order to calculate composition changes, radiative forcing and near surface temperature changes caused by these emissions. Near surface temperature change is presumed to be a reasonable indicator for climate change (Grewe and Stenke, 2008). AirClim is applicable to evaluate numerous air traffic scenarios, including different routings and technological options.

The benefit of this methodology is that the time expensive precalculations only have to be done once, and can then later be used for any AirClim simulation. A detailed description and validation is given in Grewe and Stenke (2008). Here we apply an extended AirClim version with a higher resolution, especially at mid latitudes and cruise altitudes (Fichter, 2009), and additional consideration of the climate impact of long-lived ozone reduction (O_3^{pm}) and contrail cirrus (Contrail induces cloudiness, CiC) (Appendix; Dahlmann, 2012; Grewe and Dahlmann, 2012).

2.2. Uncertainty assessment with Monte Carlo simulation

In calculating the climate impact of aviation large uncertainties exist. To ensure that the chosen mitigation option will lead to a reduction in climate impact, we consider these uncertainties in a meaningful way. In AirClim we assume

uncertainties in the following parameters to be responsible (uncertainty parameters): RF and climate sensitivity parameter (λ) for CO_2, O_3, O_3^{pm}, CH_4, H_2O, CiC, as well as the lifetimes (τ) for H_2O, O_3, O_3^{pm} and CH_4. AirClim initially used these uncertainty parameters to calculate a minimum and maximum temperature change for an individual climate agent to account for uncertainties (Grewe and Stenke, 2008). However, it is not possible to obtain the absolute minimum/maximum temperature change by simply summing minimum/maximum temperature changes caused by the different climate agents, as, for example, the climate impacts of ozone and methane are working in opposite directions. It should be noted that the uncertainties in these parameters are not statistical uncertainties, which arise from atmospheric or interannual variability, but rather uncertainties that arise from different modelling approaches, i.e. from our limited understanding of certain processes. Therefore the uncertainties are statistically not independent. For example an underestimation of CiC would lead to a lower impact in all scenarios. Due to the statistical dependence a Gaussian error propagation also is not applicable. Hence, we use a Monte Carlo (MC) simulation to obtain the uncertainty of the resulting climate impact (Fig. 1).

For the MC simulation we use the minimum and maximum of the uncertainty range of each parameter as well as a probability distribution according to literature (see Section 2.3.1 and Table 1). For the MC simulation we use 10 000 repetitions of the AirClim simulation (Fig. 1, green box) with a randomly picked value for the uncertainty parameter according to the assumed uncertainty distribution (Fig. 1, red box) and calculate RF, ΔT or other common climate metrics (CM). Thus, a broad range of possible parameter settings is calculated, leading to a sufficient uncertainty approximation according to the law of large numbers, which states, that for a large number of repetitions, the relative frequency approximates the probability of a random experiment.

Although AirClim needs only some seconds to calculate the climate impact of several scenarios on a standard desktop computer, the above described MC simulation takes a calculation time of more than one day, due to the 10 000 repetitions of the AirClim simulation. For some future applications the longer computing time might be a bottleneck. To overcome this problem we introduce a new method, in which the MC repetitions are calculated inside of AirClim (internal MC simulation). By default, AirClim provides the temperature change for a minimum and a maximum case of each uncertainty parameter (τ, RF, λ) and each individual climate agent. Hence, for each climate agent 27 different temperature changes are calculated (=3^3; 3 uncertainty parameters and 3 cases: min/mean/max). For the internal version of the MC simulation, we assume that the distribution of uncertainties is related linearly to the distribution of the resulting temperature change. Thus it is possible to use the spread between the minimum and maximum of the uncertainty parameter to obtain the spread in the resulting temperature change. If we use an uncertainty distribution with unlimited borders like normal distribution, we choose a sigma in that way that less than 0.1% of the random numbers lie outside the assumed uncertainty range (minimum and maximum value of the uncertainty range). We choose a new random number if the value lies outside of the assumed uncertainty range. For each instance of the MC simulation we first choose a random number ($\alpha_\tau(i) = [0, 1]$) for the lifetime of tropospheric and stratospheric perturbations and interpolate for each climate agent between the temperature change with minimum and maximum lifetime (τ): $\Delta T(\mathrm{RF}_*, \lambda_*) = \alpha_\tau \Delta T(\tau_{min}, \mathrm{RF}_*, \lambda_*) + (1 - \alpha_\tau)\Delta T(\tau_{max}, \mathrm{RF}_*, \lambda_*)$, where $*$ stands for the min/mean/max

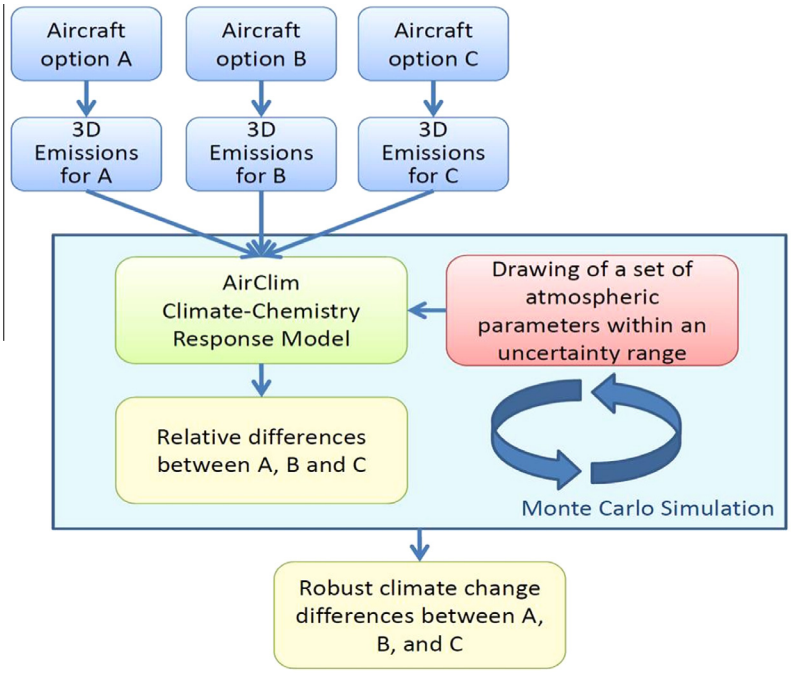

Fig. 1. Sketch of the methodology.

Table 1
Median and upper and lower limit of the uncertainty range for radiative forcing (RF) and climate sensitivity parameter (λ) for each climate agent (CO_2, H_2O, O_3, O_3^{pm}, CH_4, CiC), and error probability distribution.

		CO_2	H_2O	O_3	O_3^{pm}	CH_4	CiC
RF Grewe[a]	Distribution	Normal					
	Sigma	0.015	0.15	0.09	0.03	0.03	0.15
	Minimum	0.95	0.5	0.7	0.9	0.9	0.5
	Median	1.0	1.0	1.0	1.0	1.0	1.0
	Maximum	1.05	1.5	1.3	1.1	1.1	1.5
RF Lee[b]	Distribution	Normal	Lognormal				
	Sigma	0.135	1.20	0.68	1.09	1.09	0.47
	Minimum	0.55	0.14	0.32	0.17	0.17	0.46
	Median	1.00	1.00	1.00	1.00	1.00	1.00
	Maximum	1.45	7.25	3.13	6.10	6.10	2.17
λ[c]	Distribution	Normal					
	Sigma	0.012	0.075	0.080	0.080	0.028	0.012
	Minimum	0.69	0.58	0.70	0.70	0.77	0.39
	Median	0.73	0.83	1.00	1.00	0.86	0.43
	Maximum	0.77	1.08	1.30	1.30	0.95	0.47

[a] Grewe and Stenke (2008).
[b] Lee et al. (2009).
[c] Ponater et al. (2006), Joshi et al. (2003), and IPCC (2007).

value of the uncertainty parameters. The same is done afterwards for the uncertainty of radiative forcing (α_{RF}) and the climate sensitivity parameter (α_λ). This results in one temperature change per climate agent for each instance of the MC simulation. We limit the use of the internal MC simulation to normally distributed uncertainties as it is difficult for the user to find the right distribution parameters as well as the right minima and maxima for skewed uncertainty distributions. Therefore we show in this work generally the results for the external MC simulation. The internal MC simulation is used for a comparison of both types of MC simulations (internal and external, see Fig. 7) to show that the above assumption is valid (i.e. a linear relationship between the distribution of an uncertainty parameter and the distribution of the resulting climate impact) as well as for the use case (Section 3.3).

For quantifying the mitigation potential the crucial information is whether scenario *A* or *B* has a lower climate impact, whereas the absolute difference is less important. Therefore, we calculate (for both versions of the MC simulation) the relative difference ($\varphi_B(i)$) between the climate metric of scenario *B* ($CM_B(i)$) and a reference scenario *A* ($CM_A(i)$) for each instance *i* of the MC simulation:

$$\varphi_B(i) = \frac{CM_B(i) - CM_A(i)}{CM_A(i)}. \tag{1}$$

The reference scenario can either be one of the calculated scenarios (for example the scenario representing present-day aircraft or routing) or the mean of all calculated scenarios, depending on the question to be answered (Grewe and Dahlmann, 2015). The median and the 2.5, 25, 75 and 97.5 percentiles of the relative differences are calculated in order to quantify the uncertainty range.

To analyse the reasons for the differences between individual scenarios we split the total $\varphi_B(i)$ into components of individual climate agents: $\varphi_B(i) = \sum_{spec} \varphi_B^{spec}(i)$ with

$$\varphi_B^{spec}(i) = \frac{CM_B^{spec}(i) - CM_A^{spec}(i)}{CM_A(i)}, \tag{2}$$

where CM_B^{spec} is the climate impact of scenario *B* caused by climate agent *spec*. The benefit of calculating $\varphi_B^{spec}(i)$ relative to $CM_A(i)$ is receiving the individual contribution of each climate agent to the difference between the scenarios as additional information.

2.3. Model setup

To show the applicability of the above described uncertainty assessment we use four different emission inventories representing global air traffic emissions in different years. For comparing the climate impact of different scenarios we use the average temperature response (ATR) with a time horizon of 100 years:

$$ATR_{100} = \frac{1}{100}\int_0^{100} \Delta T(t)dt \tag{3}$$

as CM. To analyse the climate impact over more than 100 years we use emission data from Lee et al. (2009) for the historical evolution of air traffic. For future air traffic emissions we assume IPCC scenario Fa1, which is a reference scenario developed

by ICAO (International Civil Aviation Organisation) Forecasting and Economic Support Group (FESG) with midrange economic growth from IPCC (1992) and technology for both improved fuel efficiency and NO_x reduction (IPCC, 1999). For background concentrations of CO_2 and CH_4, which influence the climate impact of CO_2 and CH_4 emissions, we assume IPCC scenario A1B, which is based on the assumption of an economically oriented world with balanced use of fossil and renewable energies (Nakicenovic et al., 2000).

2.3.1. Uncertainties

For the lifetimes of tropospheric and stratospheric perturbations we assume a normal distribution for the uncertainty range of 20% and 40%, respectively (Grewe, 2007; Stevenson et al., 2006). For uncertainties of radiative forcing we use two different approximations according to Grewe and Stenke (2008) and Lee et al. (2009). Both parameter ranges are provided in Table 1. We use both assumptions and analyse the influence of the chosen uncertainty range on the resulting climate impact. It has to be noted that the uncertainty ranges given by Lee et al. (2009) are an upper limit as they include the impacts of lifetime, radiative forcing, and differences between emission inventories, while Grewe and Stenke (2008) only account for the uncertainties in radiative forcing. Nevertheless the uncertainties are not known and provide only a rough estimate. The uncertainty parameters are all assumed to be uncorrelated, except for the uncertainty of ozone and methane radiative forcings, which are highly correlated as they are both coupled with the NO_x–O_3–OH–CH_4 cycle. Studies show that for aviation, models with large ozone radiative forcing also provide large (negative) methane radiative forcing (Hoor et al., 2009; Lee et al., 2010). To account for this correlation we use in the MC simulation the same random number α_{RF} for O_3 and CH_4. Thus we assure a large ozone radiative forcing occurring with large negative methane RF. Hence, we do not fix the relation between RF(O_3) and RF(CH_4) as the relation varies due to the different uncertainty ranges.

2.3.2. Aviation emission inventories

Since mitigation options often represent small changes in emissions, we concentrate on a more generalised approach and use exemplarily four different global air traffic inventories which are normalised with regard to the total fuel consumption (AERO2k, QUANTIFY, TRADEOFF and NASA). AERO2k provides an aviation emission data set for the year 2002 for civil and military flights (Eyers et al., 2004) with a vertical resolution of 1000 ft (about 305 m). QUANTIFY emissions are based on global flight movement statistics from the Official Airline Guide (OAG) together with data of non-scheduled air traffic from the AERO2k flight database (www.pa.op.dlr.de/quantify). Total fuel consumption for the QUANTIFY dataset is scaled to the global sales data from the International Energy Agency (IEA). The vertical resolution of this emission inventory is 2000 ft (610 m). For TRADEOFF, a 1991/92 movement base year was projected to the year 2000, corrected by ICAO statistics, and converted into emissions, fuel burn and travelled distances (e.g. Gauss et al., 2006). The vertical resolution of this emission set is 2000 ft (610 m). NASA used flight movement statistics from the OAG and airline fleet databases for the year 1992 with the assumption of idealised flight routing (Baughcum et al., 1996). The vertical resolution of this data set is 1 km. As flown distances are not provided in the NASA inventory we assume the geographical distribution of flown distances according to the geographical distribution of fuel consumption, scaled to the QUANTIFY distances-fuel-ratio.

As the emission inventories differ in the calculation method as well as in the base year, they have diverse total emissions (Table 2). Thus, the climate impact of the emission inventories would be different. As we want to explore the applicability of our method for small, especially regional, differences, we use normalised emission sets by scaling the fuel consumption as well as NO_x emissions and flown distances of all scenarios to the QUANTIFY values. The remaining differences between the emission inventories are due to different distributions of the emissions with respect to latitude and altitude. Fig. 2a shows the latitudinal distributions of the emissions in percent per degree. These distributions are very similar for all inventories. All of them have high emissions between 20°N and 60°N, with a maximum at about 40°N. The altitude distribution of the emissions in percent per kft altitude (Fig. 2b) shows more variability. In the AERO2k inventory emissions are higher between 800 and 300 hPa in comparison to the other emission sets. Therefore, the maximum emission at main flight levels (200–300 hPa) is smaller in AERO2k. TRADEOFF and QUANTIFY show similar altitude profiles with relatively low emissions below 300 hPa, but a strong maximum at main flight levels at about 230 hPa. NASA provides similar emissions as TRADEOFF and QUANTIFY below 300 hPa, but a smaller maximum at 230 hPa. In contrast to the other emission sets, NASA provides more emissions above 200 hPa (up to 130 hPa) because the base year (1992) included supersonic air traffic (Concorde).

Table 2
Overview of the used emission inventories before normalisation. For our calculations we scale all emissions and flown distances to QUANTIFY values (see Scaled).

	Base year	Fuel [Tg]	NO_x [Tg_N]	Distances [10^9 km]	Vert. Resolution [m]
AERO2k	2002	176	0.68	33.2	305
QUANTIFY	2000	214	0.85	30.5	610
TRADEOFF	2000	169	0.59	25.1	610
NASA	1992	139	0.44	19.8[a]	1000
Scaled	–	214	0.85	30.5	–

[a] Flown distances are not given in the NASA dataset, but calculated by using NASA fuel distribution scaled by QUANTIFY distance-fuel-ratio.

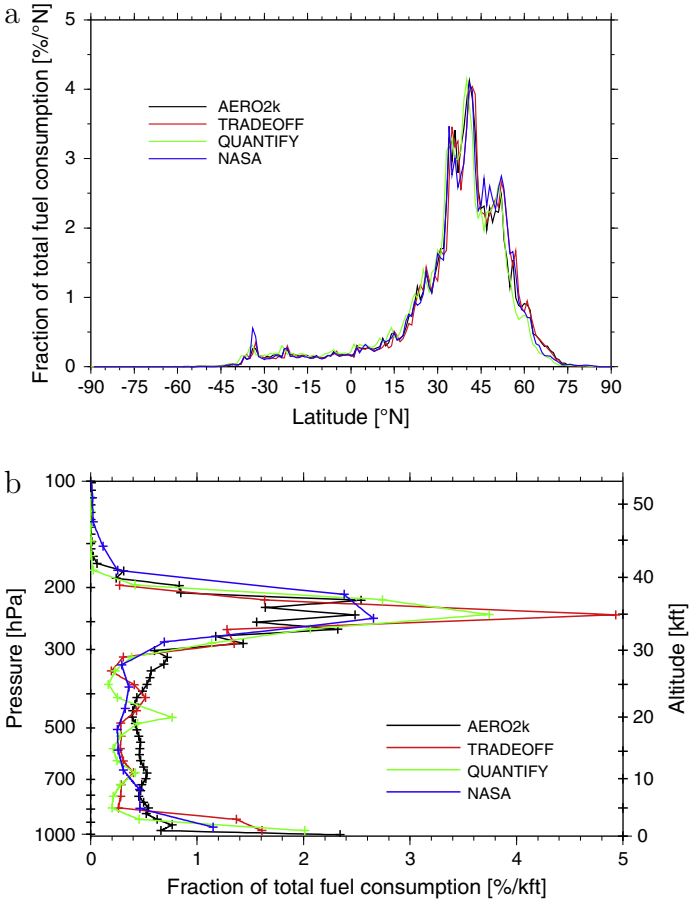

Fig. 2. Latitudinal (a) and altitudinal (b) distribution of emissions in different inventories given as density functions: AERO2k (black), TRADEOFF (red), QUANTIFY (green) and NASA (blue). (For interpretation of the references to colour in this figure legend, the reader is referred to the web version of this article.)

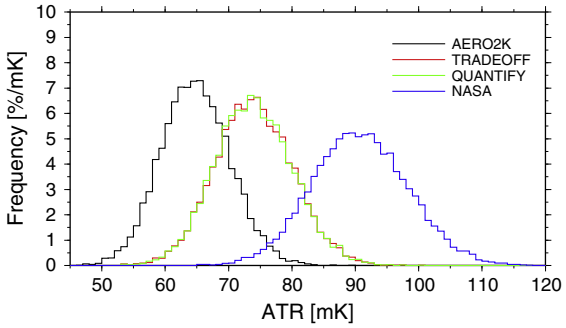

Fig. 3. Frequency density function of ATR_{100} (mK) of AERO2k (black), TRADEOFF (red), QUANTIFY (green) and NASA (blue) using the external model with the uncertainty assumptions of Grewe and Stenke (2008). (For interpretation of the references to colour in this figure legend, the reader is referred to the web version of this article.)

3. Results

3.1. Identification of changes in climate impact from different technologies

In this section we use the external MC to show the applicability of the method to identify changes in climate impact of different emission distributions. First, we analyse the ATR_{100} for the four different emission inventories, following called scenarios, with the uncertainty assumptions of Grewe and Stenke (2008) (Table 1). Due to the large uncertainty ranges, the resulting ATR_{100} distribution show a large spread (Fig. 3). The ATR_{100} caused by the AERO2k emission inventory, for example

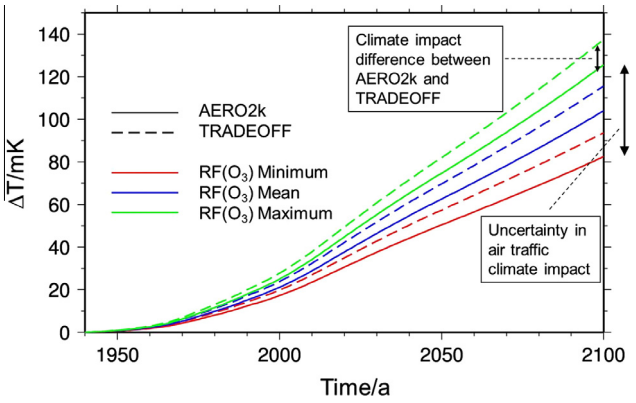

Fig. 4. Temperature change (mK) caused by the TRADEOFF and QUANTIFY emission inventories with different RF values for ozone (green: maximum RF, blue: mean RF, red: minimum RF). The arrows indicate ranges for the uncertainty in the air traffic climate impact caused by changes in ozone RF (large arrow) and the difference between climate impact from two emission inventories (small arrow). (For interpretation of the references to colour in this figure legend, the reader is referred to the web version of this article.)

varies between about 50 and 80 mK. Due to this large spread the ATR_{100} caused by the different scenarios do not differ significantly on a 95% confidence level except for AERO2k and NASA. However, this approach ignores that the uncertainties which are assessed here are not statistical uncertainties, which arise from atmospheric or interannual variability, but rather uncertainties that arise from different modelling approaches, representing atmospheric uncertainties. Hence, we analyse pairwise relative differences of the ATR_{100} of two scenarios for individual sets of uncertainty parameters, which is demonstrated in Fig. 4. The figure shows the temporal evolution of two scenarios for three different assumptions (instances) for the strength of ozone radiative forcing. The large arrow indicates the uncertainty range for the total climate impact of aviation due to uncertainties of ozone radiative forcing. The small arrow indicates the difference in the climate impact from two emission inventories. While the uncertainty in absolute temperature change is large, the relative difference for each of the assumptions is quite similar (about 9–14%).

In Fig. 5 the percentiles of the distribution of relative differences (φ, Eq. (1)) of an individual scenario to the mean of all scenarios are provided (grey bars). Despite the large uncertainty in the total ATR_{100} calculation and the normalised emissions, at least three of the scenarios can be distinguished on a 95% confidence level with this kind of assessment. Only the climate impacts of TRADEOFF and QUANTIFY emission inventories cannot be distinguished on a 95% confidential interval. Thus, the climate impact caused by the NASA inventory is 20% higher than the average of all scenarios, while the climate impact caused by the AERO2k inventory is 15% smaller.

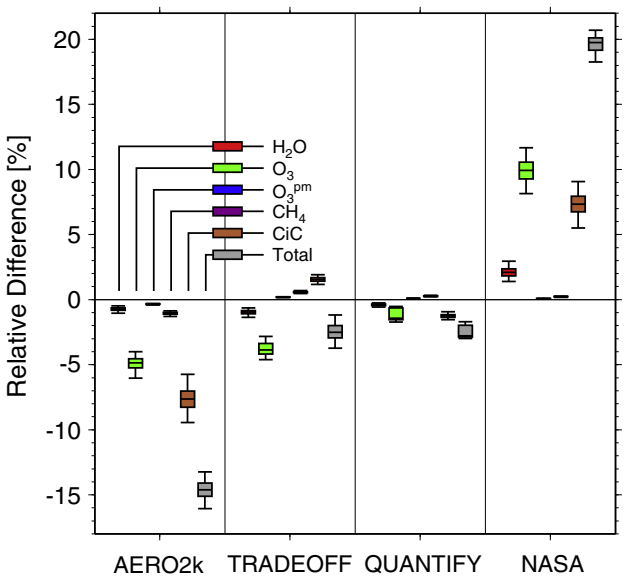

Fig. 5. Relative pairwise difference (φ and φ^{spec}) between climate impacts of the AERO2k, TRADEOFF, QUANTIFY and NASA emission inventories and the mean of all scenarios as calculated by the external model with the uncertainty assumptions of (Grewe and Stenke, 2008). Boxes indicate the 25 and 75 percentile and the whiskers indicate the 2.5 and 97.5 percentiles.

To analyse the reason for the differences between the scenarios we split the relative differences into contributions of the different climate agents (φ^{spec}, Eq. (2), Fig. 5). The 20% higher climate impact from the NASA emission inventory is mainly caused by the impact of O_3, CiC, and H_2O, which cause a difference of about 10%, 7%, and 2%, respectively. The impacts of CH_4 and O_3^{pm} have only minor contributions to the total differences. NASA provides emissions up to higher altitudes than the other emission inventories (Fig. 2b). This leads to the higher impact of ozone, contrail cirrus, and water vapour compared to the other emission scenarios, as the climate impact of ozone, contrail cirrus and water vapour increases strongly with increasing altitude. There is no difference in the climate impact of CO_2 between the different emission inventories, as they are normalised to the same fuel consumption and the climate impact of CO_2 does not depend on the emission location. The AERO2k inventory shows the lowest climate impact (−15%), mainly due to lower impacts of contrail cirrus (−8%) and ozone (−5%). The other climate agents contribute around or less than −1% to the difference. The lower climate impact of AERO2k from ozone and contrail cirrus is caused by low emissions at higher altitudes and increased emissions at lower altitudes, where the climate impacts of ozone, water vapour, and contrails are generally small because of small lifetimes of water vapour and ozone precursors as well as too warm temperatures for contrail formation. The climate impact of the TRADEOFF inventory is only about 2% smaller than the mean of all scenarios, as the smaller impacts of ozone and water vapour are partly compensated by the higher climate impact of the contrails. Compared to NASA, TRADEOFF provides emissions in lower altitudes, leading to a lower impact of ozone and water vapour. The higher climate impact of CiCc is caused by higher emissions at the main flight level (about 230 hPa), which causes a larger ontrail-cirrus coverage. The relative differences of the other climate agents are positive, but less than 1%. The climate impact of QUANTIFY emissions is almost the same as for TRADEOFF (−3%) but with different contribution from the individual climate agents. QUANTIFY shows higher climate impact of ozone and water vapour due to emissions up to higher altitudes compared to TRADEOFF, compensated by lower climate impact of contrail cirrus due to a smaller emission maximum at the main flight level (230 hPa).

The results presented above were calculated using the uncertainty assumptions of Grewe and Stenke (2008). To analyse to which extent the results depend on the choice of uncertainty ranges, we performed a second MC simulation with uncertainty assumptions from Lee et al. (2009) and compare the results of both assumptions in Fig. 6. The medians of the relative differences of an individual scenario to the mean of all scenarios for both uncertainty assumptions differ by less than 0.5 percentage points for each of the emissions scenarios. As the uncertainty ranges given in Lee et al. (2009) are larger than in Grewe and Stenke (2008), the uncertainties in the resulting temperature changes are also larger. Note that the RF uncertainty ranges given by Lee et al. (2009) provide an upper limit estimate (see above). The uncertainty range for NASA, for example, is four times larger when using the Lee et al. (2009) assumption than it is when using the Grewe and Stenke (2008) assumption. Due to the larger uncertainty, TRADEOFF can no longer be distinguished significantly on a 95% confidence level from the mean of all scenarios. Nevertheless, the conclusion that the NASA inventory leads to about 20% larger and the AERO2k dataset to about 14% lower climate impact than the mean of all scenarios remains unchanged.

3.2. A fast identification method for time-consuming use cases

To analyse the applicability of the internal MC version, we performed an additional internal MC simulation with the uncertainty assumptions according to Grewe and Stenke (2008). The comparison of the internal and the external model

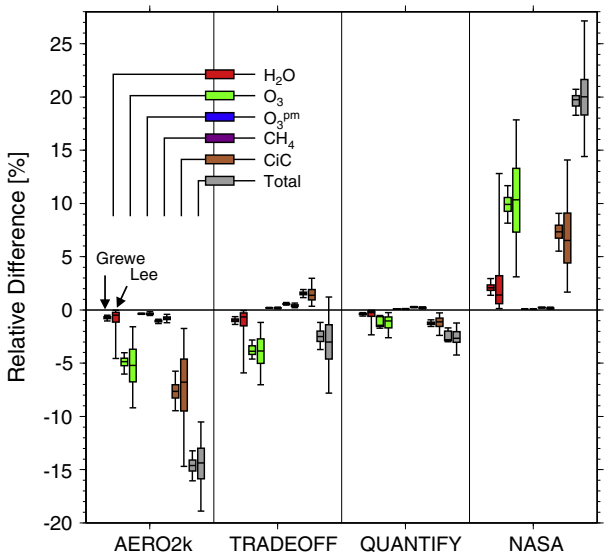

Fig. 6. Comparison of relative differences (φ and φ^{spec}) between climate impacts of the AERO2k, TRADEOFF, QUANTIFY and NASA emission inventories and the mean of all scenarios. Calculated with the external model with the uncertainty assumptions of Grewe and Stenke (2008, left) and Lee et al. (2009, right), respectively. Boxes indicate the 25 and 75 percentile and the whiskers indicate the 2.5 and 97.5 percentiles.

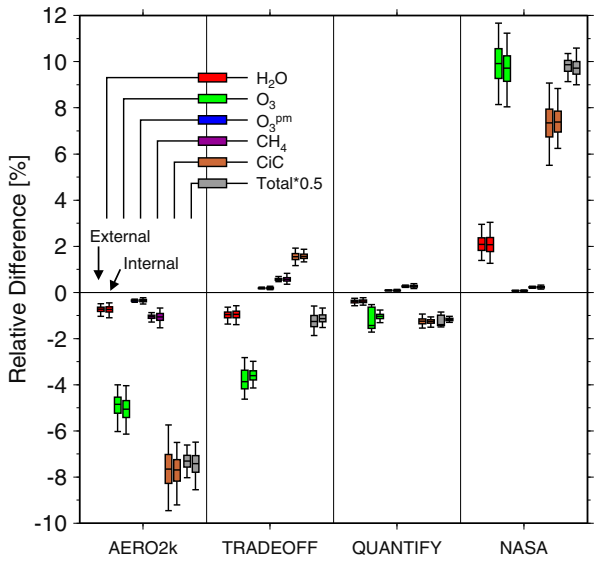

Fig. 7. Comparison of relative differences (φ and φ^{spec}) between climate impacts of the AERO2k, TRADEOFF, QUANTIFY and NASA emission inventories and the mean of all scenarios calculated with the external model (left) and the internal model (right) with the uncertainty assumptions of Grewe and Stenke (2008). Boxes indicate the 25 and 75 percentile and the whiskers indicate the 2.5 and 97.5 percentiles. For visibility reasons we scaled the total climate impact by 0.5.

results is displayed in Fig. 7. Although there are minor differences, both model versions provide qualitatively the same results. The uncertainties of the internal model version are smaller for the TRADEOFF and QUANTIFY inventories, but larger for NASA and AERO2k. These differences are mainly caused by the uncertainties in τ (lifetime of tropospheric and stratospheric perturbations), as this has a nonlinear effect on temperature change. If we neglect uncertainties in τ, both model versions provide almost identical results (not shown).

3.3. TRADEOFF – a use case

As a use case we analyse the mitigation gain of shifting air traffic by 2000 ft up or 2000, 4000 or 6000 ft down, respectively (about 610, 1220 and 1830 m) as it was done in the TRADEOFF project (e.g. Frömming et al., 2012). For these mitigation scenarios aircraft increase or decrease their mean flight altitude if they are able to perform these flight profiles. Changes in fuel consumption as well as NO_x emission due to changed flight altitude are taken into account (see Table 3).

The relative changes of the mitigation scenarios to the base case in terms of ATR_{100} using the internal MC simulation are shown in Fig. 8. For an increase of mean flight altitude by 2000 ft fuel consumption decreases by 0.6% leading to a decrease in climate impact due to CO_2 by 0.2%. However, the total climate impact increases by about 8.5% as the emissions take place in more climate sensitive regions (see Fig. A.2). The increase in climate impact is mainly due to O_3 and CiC (+5.0% and +2.3%, respectively). In contrast, a reduction of mean flight altitude increases the fuel consumption and thus the impact of CO_2. Nevertheless the total climate impact decreases with mean flight altitude as the decrease of O_3 and CiC dominates the increase of CO_2. A reduction in flight altitude by 6000 ft reduces the overall climate impact by 23%. Despite the large uncertainties the mitigation scenarios with changes flight altitudes provide significantly higher or lower climate impact compared with the base case.

The results provided here are not directly comparable to those from Frömming et al. (2012) as different models and metrics are used. In AirClim we use ATR_{100} while Frömming et al. (2012) uses RF and ΔT in 2100. In addition we account for CiC while Frömming et al. (2012) only account for linear contrails which are about nine times smaller as CiC (Burkhardt and

Table 3
Annual mean fuel consumption and emissions for TRADEOFF base scenario and flight altitude changes.

	Fuel consumption Tg/a	NO_x emissions Tg(N)/a	Flown Distances 10^9 km/a
+2000 ft	151	0.61	25.4
Base	152[a]	0.60	25.4
−2000 ft	156	0.62	25.4
−4000 ft	160	0.63	25.4
−6000 ft	161	0.63	25.4

[a] Different from Table 2 as no military emissions are included.

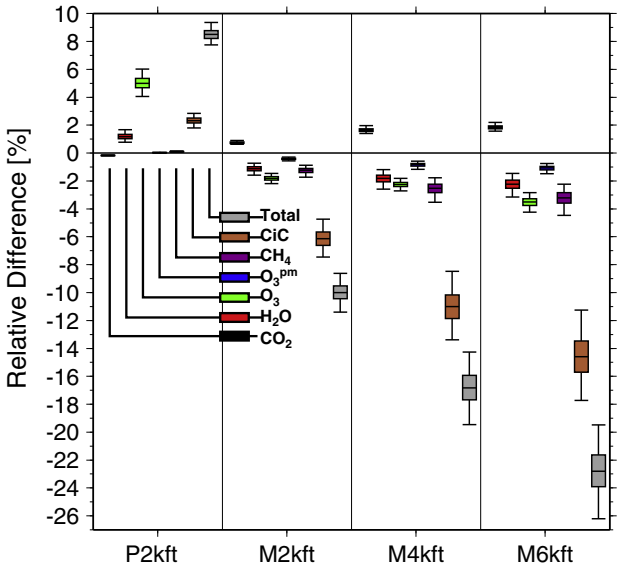

Fig. 8. Relative difference between TRADEOFF mitigation scenarios and TRADEOFF base case with uncertainty assumptions of Grewe and Stenke (2008) and the internal MC simulation. Boxes indicate the 25 and 75 percentile and the whiskers indicate the 2.5 and 97.5 percentiles.

Kärcher, 2011). If we only consider the impact of linear contrails, total climate impact in terms of ΔT in 2100 would be reduced by about 12% for the scenario with 4000 ft lower flight altitudes (not shown), which is in agreement with 17% in Frömming et al. (2012).

4. Conclusion

In this paper we presented a methodology to analyse the climate impact (i.e. the average temperature response over 100 years) of different air traffic scenarios and the influence of different uncertainty estimates. As the uncertainties in assessing the climate impact of aviation are large, the calculated temperature change shows a wide spread. We calculated the relative difference of climate impacts between different emission scenarios for many possible combinations of uncertainty parameters. We found significant differences between most of the scenarios, although the emission inventories were very similar. This shows that it is often possible to determine significant differences between the climate impacts of differing emission data sets. Thus it is possible to obtain a reliable assessment, although considerable uncertainties in the overall climate impact exist. In addition this study shows that the knowledge of the exact emission region is particularly important to accurately determine the climate impact of air traffic.

The application of AirClim within a Monte Carlo simulation shows that a variety of mitigation options can be assessed and analysed with respect to significant differences in climate impact. Due to its numerical efficiency, the method can be used for air traffic optimisation studies. For instance, an analysis and optimisation of the climate mitigation gain by changing the operation point (speed and cruise altitude) of present-day aircraft is presented in Koch (2013).

Acknowledgments

This work was performed within the DLR projects “Climate-compatible air transport system (CATS)” and ”WeCare”.

Appendix A. AirClim 2.0: Model description

A.1. Overview

AirClim is a response model, i.e. it uses the relation between emissions of CO_2, NO_x and H_2O and their impacts on atmospheric composition with respect to carbon dioxide, ozone, methane, water vapour, and contrails. The AirClim model version 1.0 is documented in Grewe and Stenke (2008). That version was developed for supersonic air traffic and included effects from emissions of CO_2, H_2O, NO_x and flight distance on the radiative forcing and the global mean near surface temperature changes via the climate agents CO_2, H_2O, O_3 (stratospheric and tropospheric), CH_4 and line-shaped contrails. The model was updated in Dahlmann (2012) based on model simulations from Fichter (2009) and Burkhardt and Kärcher (2009). The updated version makes use of an enhanced vertical and horizontal resolution (including subsonic air traffic) and includes

contrail-cirrus, and primary mode ozone (O_3^{pm}), i.e., the effect of changes in methane on ozone. A complex process model is used to produce a large set of relations between an emission at a particular location and its effect on climate (emission–effect relations). For chemical changes and the associated RF Appendices (A.2) and (A.3) the simulations were performed with the climate-chemistry model E39/CA and were analysed in Fichter (2009). For contrail-cirrus (CiC, A.4), the base model is ECHAM4-CCMod (Burkhardt and Kärcher, 2009, 2011).

A.2. Resolution AirClim 2.0 for subsonic air traffic

The resolution of AirClim is given by the number of pre-calculated emission–effect relations. 85 simulations were performed. One base case simulation with E39/CA, which includes state-of-the art emissions for all categories, such as industry, biomass burning, and air traffic, and 84 simulations with a constant flux of NO_x and H_2O (same value as in Grewe and Stenke (2008)) is added in one of the latitude/altitude regions (=red boxes in Fig. A.1, 7 latitude bands and 12 altitude ranges). The difference of each of the 84 simulations to the base case simulation is the increase in concentration of atmospheric species due to this additional emission (see Appendix A.3). Hence for the chemistry effects the resolution of AirClim varies between 15° latitude and 30° latitude, with a higher resolution in northern mid latitudes, where most air traffic occurs. The vertical resolution varies also and has a resolution of roughly 1 km. Cruise altitudes for most subsonic aircraft are usually located between 300 hPa and 200 hPa.

A.3. Chemistry

The response of a local emission to the global and annual mean water vapour, ozone, methane and contrail induced cirrus radiative forcing is shown in Fig. A.2 given as global mean RF per unit emission or flown distance. The figures are consistent with Grewe and Stenke (2008), but have a much higher internal vertical and horizontal resolution.

Changes in the methane concentration affect the HO_x ($OH + HO_2$) partitioning, e.g. a lower methane concentration reduces the reaction rate of $CH_4 + OH \rightarrow CH_3 + H_2O$ and a subsequent production of HO_2, which reduces the reaction rate of the rate limiting reaction of tropospheric ozone production $NO + HO_2 \rightarrow NO_2 + OH$. Hence a decrease in methane due to air traffic emissions feeds back to the ozone concentration (less ozone production). This effect is much smaller than the initial ozone production and the lifetime of this ozone change is bounded to the methane perturbation. This ozone change is called primary mode ozone (O_3^{pm}). Simulations with E39/CA show a factor between the RF of methane and O_3^{pm} of 0.29. Hence, this effect is included in AirClim via $RF(O_3^{pm}) = 0.29 \cdot RF(CH_4)$.

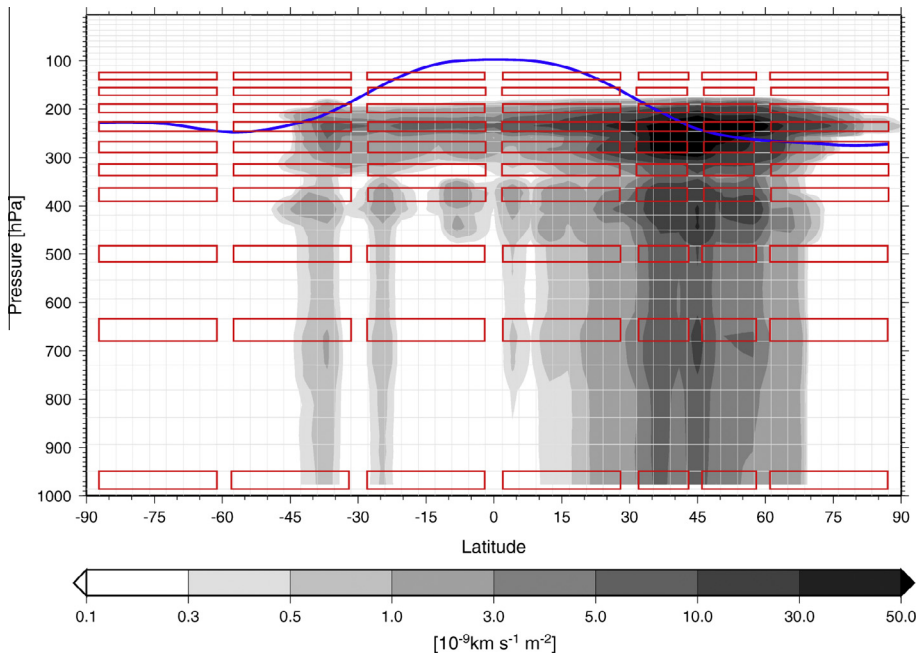

Fig. A.1. Positions of the emission regions of the idealised emission scenarios (red boxes). In the background, exemplarily annual flight distance densities from global aviation are shown in km/s/kg (air). The tropopause is shown in blue. From Fichter (2009). (For interpretation of the references to colour in this figure legend, the reader is referred to the web version of this article.)

A.4. Contrail-Cirrus

A multi-annual simulation using the AERO2k inventory with ECHAM4-CCMod (Burkhardt and Kärcher, 2009, 2011) was analysed to deduce a relation between flown distances and the RF of CiC. A three step approach was found to have reasonable correlation (Dahlmann, 2012).

1. Flown distance + Schmidt-Appleman Criterion → Contrail-flight distance density
2. Contrail-flight distance density + Ice Supersaturation → Contrail coverage
3. Contrail coverage → RF(CiC)

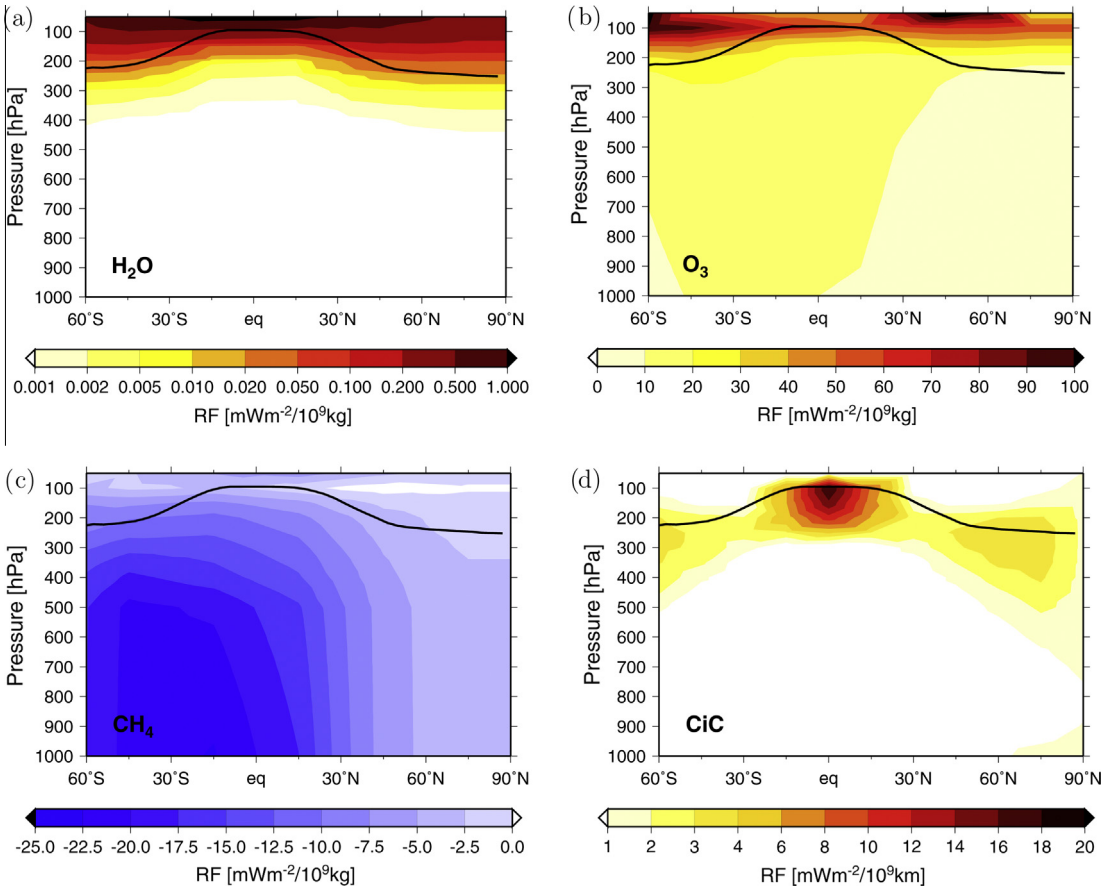

Fig. A.2. Global and annual mean radiative forcing of H_2O, O_3, CH_4 and CiC as a function of emission location.

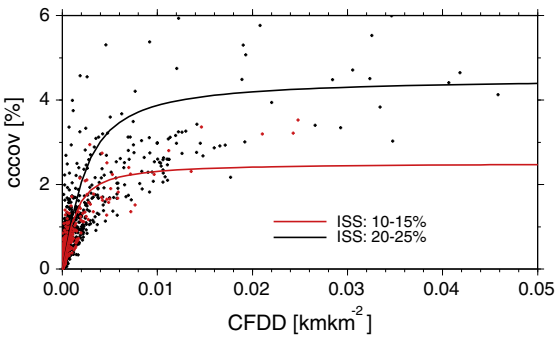

Fig. A.3. Correlation between CFDD and cccov for two different regimes of ice super saturation. The crosses represent data from the climate model and lines provide the best fit.

To obtain CiC radiative forcing, as a first step, the weighted sum of the flown distance in a grid box is calculated. The local weight is the probability that the Schmidt-Appleman Criterion (SAC) is fulfilled (p_{SAC}), which is derived from the climate model ECHAM4-CCMod (Burkhardt et al., 2008). The contrail-flight distance density (CFDD) is then

$$\mathrm{CFDD}(i,j) = \sum_k \left(\frac{\text{Flown Distance}(i,j,k)}{\text{Grid Area}(i,j)} \cdot p_{SAC}(i,j,k) \right). \tag{A.1}$$

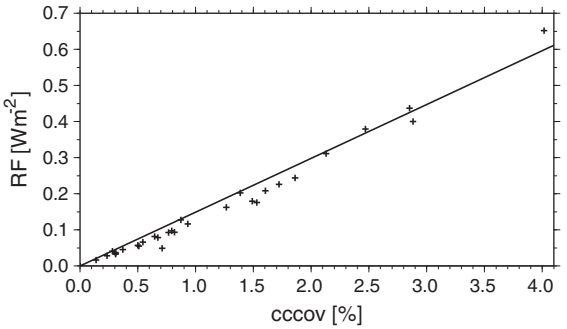

Fig. A.4. Correlation between radiative forcing and contrail coverage with an optical depth of 0.02. Crosses represent climate model data and the line represents the best fit.

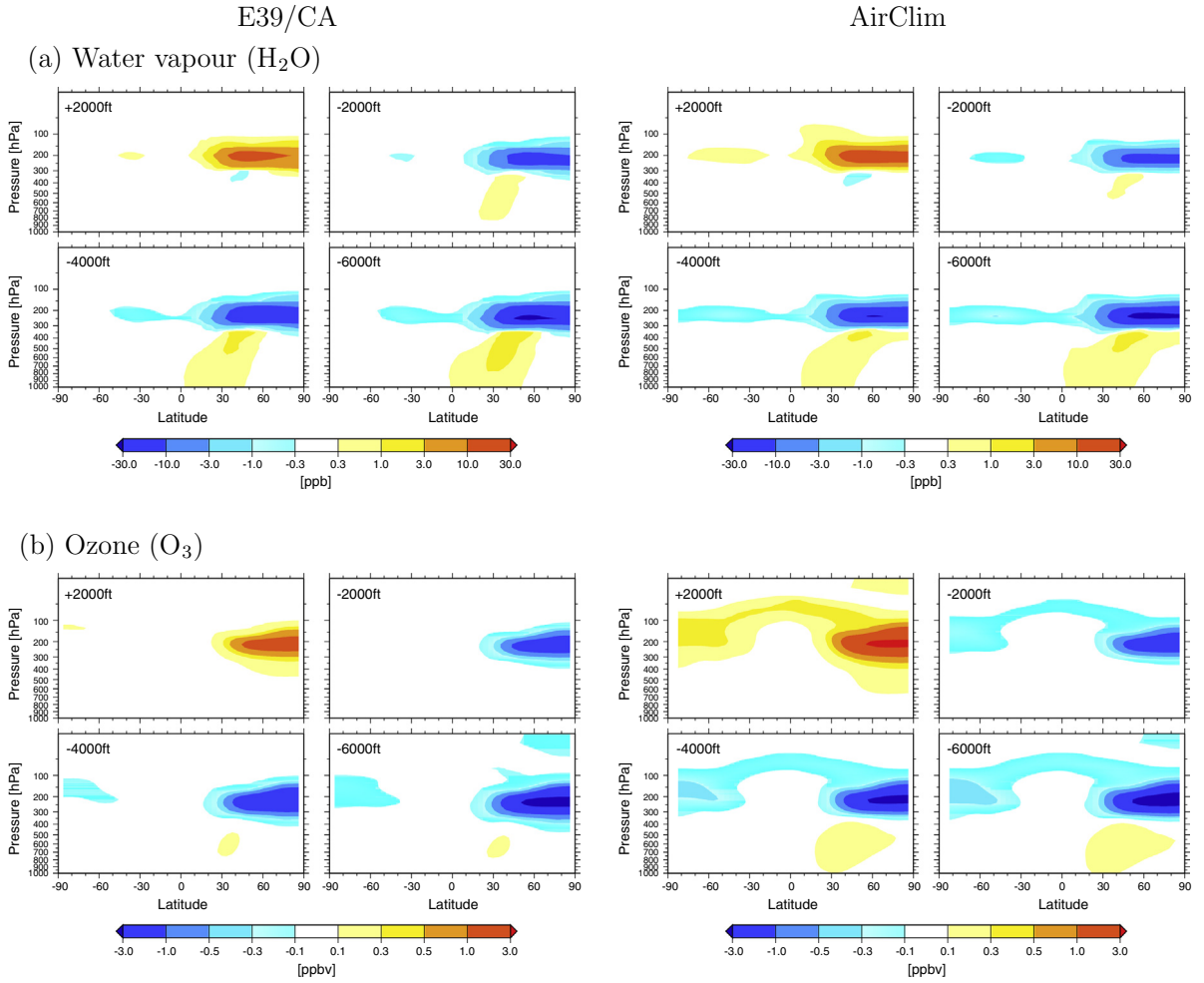

Fig. A.5. Comparison of changes in (a) water vapour mixing ratio and (b) ozone mixing ratio through changes of mean flight altitudes as determined by the complex climate chemistry model E39/CA (left) and the climate response model AirClim (right) (from Fichter (2009)).

Here, i, j, k are the grid indices for longitude, latitude and level. For the second step additional climate model simulations were performed with year 2002 air traffic and fivefold year 2002 air traffic to obtain a larger parameter space. The fractional area of ice super saturation (ISS) as well as the contrail cirrus coverage with an optical depth larger than 0.02 in the shortwave (cccov) for every horizontal grid (i, j) was calculated by the climate model. For ISS as well as cccov we assume maximum random overlap between 200 and 250 hPa. The resulting response function between contrail-flight distance density, ice super saturation and contrail coverage derived by fitting climate model data, is then:

$$\mathrm{cccov}(i,j) = 0.128 \cdot \mathrm{ISS}(i,j) \cdot \arctan\left(97.7 \cdot \frac{\mathrm{CFDD}(i,j)}{\mathrm{ISS}(i,j)}\right). \tag{A.2}$$

The results are shown in Fig. A.3 for two different ranges of ice super saturation.

The last step is again based on a correlation derived from the contrail-cirrus simulations:

$$\mathrm{RF} = 14.9\ \mathrm{W\,m^{-2}} \cdot \overline{\mathrm{cccov}}. \tag{A.3}$$

Here $\overline{\mathrm{cccov}}$ is the global mean coverage derived from all horizontal grid boxes ($\mathrm{cccov}(i,j)$). The correlation is shown in Fig. A.4.

A.5. Validation

A.5.1. Comparison response model – complex model

Fichter (2009) analysed the difference between AirClim results and results from the complex model E39/CA for the TRADEOFF scenarios where flight altitudes were shifted by 2000 ft up or 2000, 4000 and 6000 ft down, respectively. Fig. A.5 shows the differences of the base case to the respective perturbation case for all species for the complex model (left) and the response model (right). Fig. A.5a shows, that the zonal mean perturbation of H_2O concentration agrees well between AirClim and E39/CA and the difference in the global mean RF is less than 3%. The zonal mean O_3 perturbation from AirClim shows a larger spread toward the southern hemisphere in comparison to E39/CA (Fig. A.5b). The ozone as well as the methane RF is 33 and 31% higher in AirClim compared to E39/CA. Reasons for the differences could be the lower spatial resolution in AirClim or nonlinearities.

The global mean contrail cirrus RF for global air traffic in 2002 (AERO2k) calculated with a complex climate model (ECHAM4-CCMod) is 37.5 mW m^{-2} (Burkhardt and Kärcher, 2011). AirClim calculates identical global contrail cirrus

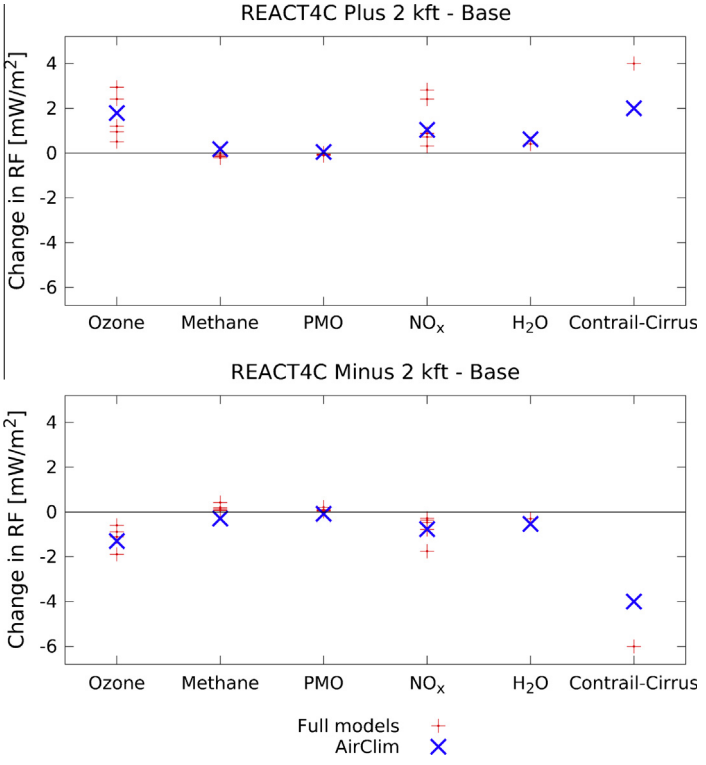

Fig. A.6. Change in RF of different species for a change of flight altitudes by 2000 ft up or down as calculated in the REACT4C project by means of several complex models in comparison with AirClim results.

coverage of 0.23% for the same emissions, but a 9% lower RF (34.2 mW m^{-2}). One reason for this difference could be the fact, that AirClim account for latitude dependency of contrail cirrus coverage but not for the latitude dependency of the RF per cccov. To analyse how well AirClim reproduces saturation effects occurring for CiC, three additional simulations with scaled air traffic (factor of 0.5, 2 and 5) were performed. AirClim shows quite similar saturation effects as ECHAM4-CCMod with differences less than 8% between the two models. However, this CiC calculation is only tested for emission distributions similar to present-day air traffic. If future air traffic is shifted, for example, to the tropics this calculation may lead to errors as the CiC RF is not only dependent on contrail cirrus coverage, but also on optical depth which varies with altitude and latitude.

A.5.2. Comparison of AirClim and other climate models

The comparison of AirClim with other climate models shows good agreement. The change in global mean RF for several species for a change of flight altitudes by 2000 ft up or down for different complex climate chemistry models compared to AirClim is shown in Fig. A.6 (REACT4C, Søvde et al. (2014), Matthes et al. (2015), Lim et al. (2015)). Qualitatively both model types provide the same results, only for methane they differ in sign. However the methane RF is small and has only a minor influence on the total climate impact.

References

Baughcum, S.L., Tritz, T.G., Henderson, S.C., Pickett, D.C., 1996. Scheduled Civil Aircraft Emission Inventories for 1992: Database Development and Analysis. NASA-CR-4700, National Aeronautics and Space Administration, Langley Research Center, Hampton, VA, USA, 196pp.

Burkhardt, U., Kärcher, B., 2009. Process-based simulation of contrail cirrus in a global climate model. J. Geophys. Res. 114, D16201.

Burkhardt, U., Kärcher, B., 2011. Global radiative forcing from contrail cirrus. Nat. Clim. Change 1, 54–58.

Burkhardt, U., Kärcher, B., Ponater, M., Gierens, K., Gettelman, A., 2008. Contrail cirrus supporting areas in model and observations. Geophys. Res. Lett. 35.

Dahlmann, K., 2012. Eine Methode zur effizienten Bewertung von Manahmen zur Klimaoptimierung des Luftverkehrs. Ph.D. thesis. Fak. für Phys., Ludwigs-Maximilians-Universität München.

Dahlmann, K., Grewe, V., Ponater, M., Matthes, S., 2011. Quantifying the contributions of individual NO_x sources to the trend in ozone radiative forcing. Atmos. Environ. 45, 2860–2868.

Eyers, C.J., Norman, P., Middel, J., Plohr, M., Michot, S., Atkinson, K., Christou, R.A., 2004. AERO2K Global Aviation Emissions Inventories for 2002 and 2025. QinetiQ. Project report 04/01113.

Fichter, C., 2009. Climate Impact of Air Traffic Emissions in Dependency of the Emission Location. Ph.D. thesis. Manchester Metropolitan University.

Frömming, C., Ponater, M., Dahlmann, K., Grewe, V., Lee, D., Sausen, R., 2012. Aviation-induced radiative forcing and surface temperature change in dependency of the emission altitude. J. Geophys. Res. D: Atmos. 117.

Gauss, M., Myhre, G., Isaksen, I.S.A., Grewe, V., Pitari, G., Wild, O., Collins, W.J., Dentener, F.J., Ellingsen, K., Gohar, L.K., 2006. Radiative forcing since preindustrial times due to ozone changes in the troposphere and the lower stratosphere. Atmos. Chem. Phys. 6, 575–599.

Grewe, V., 2007. Impact of climate variability on tropospheric ozone. Sci. Total Environ. 374, 167–181.

Grewe, V., Dahlmann, K., 2012. Evaluating climate-chemistry response and mitigation options with airclim. In: Schumann, U. (Ed.), Atmospheric Physics: Background – Methods – Trends. Springer Verlag, Berlin, Heidelberg, pp. 591–606.

Grewe, V., Dahlmann, K., 2015. How ambiguous are climate metrics? and are we prepared to assess and compare the climate impact of new air traffic technologies? Atmos. Environ. 106, 373–374.

Grewe, V., Dameris, M., Fichter, C., Lee, D., 2002a. Impact of aircraft NO_x emissions. Part 2: effects of lowering the flight altitude. Meteorol. Z. 11, 197–205.

Grewe, V., Dameris, M., Fichter, C., Sausen, R., 2002b. Impact of aircraft NO_x emissions, Part 1: interactivly coupled climate-chemistry simulations and sensitivities to climate-chemistry feedback, lightning and model resolution. Meteorol. Z. 3, 177–186.

Grewe, V., Stenke, A., 2008. AirClim: an efficient climate impact assessment tool. Atmos. Chem. Phys. 8, 4621–4639.

Grooß, J.U., Brühl, C., Peter, T., 1998. Impact of aircraft emissions on tropospheric and stratospheric ozone. Part I: chemistry and 2-D model results. Atmos. Environ. 32, 3152–3184.

Hoor, P., Borken-Kleefeld, J., Caro, D., Dessens, O., Endresen, O., Gauss, M., Grewe, V., Hauglustaine, D., Isaksen, I.S.A., Jöckel, P., 2009. The impact of traffic emissions on atmospheric ozone and OH: results from QUANTIFY. Atmos. Chem. Phys. 9, 3113–3136.

ICAO, 2013. International Civil Aviation Organization, Global Air Transport Outlook to 2030 and trends to 2040. Montreal. Circular 333, AT/190.

IPCC, 1992. In: Houghton, J.T., Callander, B.A., Varney, S.K. (Eds.), WMO/UNEP, Cambridge University Press, Cambridge, UK, 200pp.

IPCC, 1999. Aviation and the global atmosphere and a special report of IPCC working groups I and III. Intergovernmental Panel on Climate Change. Cambridge University Press, Cambridge, UK and New York, NY, USA.

IPCC, 2007. Climate Change 2007: The Physical Science Basis. Cambridge University Press, New York, USA.

IPCC, 2013. Climate change 2013: the physical science basis. Contribution of Working Group I to the Fifth Assessment Report of the Intergovernmental Panel on Climate Change. Cambridge University Press, Cambridge, United Kingdom and New York, NY, USA.

Joshi, M., Shine, K., Ponater, M., Stuber, N., 2003. A comparison of climate response to different radiative forcings in the general circulation models: toward an improved metric of climate change. Clim. Dyn. 20, 843–854.

Koch, A., 2013. Climate Impact Mitigation Potential Given by Flight Profile and Aircraft Optimization. Ph.D. Thesis. Technische Universität Hamburg-Harburg. DLR-Forschungsbericht 2013-37.

Köhler, M.O., Rädel, G., Dessens, O., Shine, K.P., Rogers, H.L., Wild, O., Pyle, J.A., 2008. Impact of perturbations to nitrogen oxide emissions from global aviation. J. Geophys. Res. 113, 4175.

Köhler, M.O., Rädel, G., Shine, K.P., Rogers, H.L., Pyle, J.A., 2013. Latitudinal variation of the effect of aviation nox emissions on atmospheric ozone and methane and related climate metrics. Atmos. Environ. 64, 1–9.

Lacis, A., Wuebbles, D.J., Logen, J.A., 1990. Radiative forcing of climate by changes in vertical distribution of ozone. J. Geophys. Res. 95, 9971–9981.

Lee, D., Pitari, G., Grewe, V., Gierens, K., Penner, J., Petzold, A., Prather, M., Schumann, U., Bais, A., Berntsen, T., Iachetti, D., Lim, L., Sausen, R., 2010. Transport impacts on atmosphere and climate: aviation. Atmos. Environ. 44, 4678–4734, Transport Impacts on Atmosphere and Climate: The ATTICA Assessment Report.

Lee, D.S., Fahey, D.W., Forster, P.M., Newton, P.J., Wit, R.C.N., Lim, L.L., Owen, B., Sausen, R., 2009. Aviation and global climate change in the 21st century. Atmos. Environ. 43, 3520–3537.

Lim, L., Lee, D., Matthes, S., Burkhardt, U., Dietmüller, S., Iachetti, D., Isaksen, I., Owen, B., Pitari, G., Skowron, A., Søvde, O., 2015. React4c: simplified mitigation studies. In: Proceedings of the 4th International Conference on Transport, Atmosphere and Climate (TAC-4).

Matthes, S., Søvde, O., Lim, L., Dietmüller, S., Skowron, A., Iachetti, D., Pitari, G., 2015. The global impact of weather-dependent climate-optimal tracectories in the north atlantic. In: Proceedings of the 4th International Conference on Transport, Atmosphere and Climate (TAC-4).

Nakicenovic, N., Alcamo, J., Davis, G., de Vries, B., Fenhann, J., Gaffin, S., Gregory, K., Grubler, A., Jung, T.Y., Kram, T., La Rovere, E.L., Michaelis, L., Mori, S., Morita, T., Pepper, W., Pitcher, H.M., Price, L., Riahi, K., Roehrl, A., Rogner, H.H., Sankovski, A., Schlesinger, M., Shukla, P., Smith, S.J., Swart, R., van Rooijen,

S., Victor, N., Dadi, Z., 2014. Special Report on Emissions Scenarios: a special report of Working Group III of the Intergovernmental Panel on Climate Change. Cambridge University Press, New York, NY (US).
Newinger, C., Burkhardt, U., 2012. Sensitivity of contrail cirrus radiative forcing to air traffic scheduling. J. Geophys. Res.: Atmos., 117
Ponater, M., Pechtl, S., Sausen, R., Schumann, U., Hüttig, G., 2006. Potential of the cryoplane technology to reduce aircraft climate impact: a state-of-the-art assessment. Atmos. Environ.
Rädel, G., Shine, K.P., 2008. Radiative forcing by persistent contrails and its dependence on cruise altitudes. J. Geophys. Res. 113, D07105.
Sausen, R., Gierens, K., Ponater, M., Schumann, U., 1998. A diagnostic study of the global distribution of contrails part i: present day climate. Theoret. Appl. Climatol. 61, 127–141. http://dx.doi.org/10.1007/s007040050058.
Schumann, U., 1996. On conditions for contrail formation from aircraft exhausts. Meterol. Z. 5, 4–23.
Schumann, U., 2000. Influence of propulsion efficiency on contrail formation. Aerosp. Sci. Technol. 4, 391–401 (11).
Søvde, O., Matthes, S., Skowron, A., Iachetti, D., Lim, L., Owen, B., Hodnebrog, T., Di Genova, G., Pitari, G., Lee, D., Myhre, G., Isaksen, I., 2014. Aircraft emission mitigation by changing route altitude: a multi-model estimate of aircraft nox emission impact on o3 photochemistry. Atmos. Environ. 95, 468–479.
Stenke, A., Grewe, V., Ponater, M., 2008. Lagranian transport of water vapor and cloud water in the ECHAM4 GCM and its impact on the cold bias. Clim. Dyn. 31, 491–506.
Stevenson, D.S., Dentener, F.J., Schultz, M.G., Ellingsen, K., van Noije, T.P.C., Wild, O., Zeng, M., Amann, G., Atherton, C.S., Bell, N., 2006. Multimodel ensemble simulations of present-day and near-future tropospheric ozone. J. Geophys. Res. 111, D08301.
Stuber, N., Ponater, M., Sausen, R., 2005. Why radiative forcing might fail as a predictor of climate change. Clim. Dyn. 24, 497–510.
Williams, J.E., Hodnebrog, T., van Velthoven, P.F.J., Berntsen, T.K., Dessens, O., Gauss, M., Grewe, V., Isaksen, I.S.A., Olivia, D., Prather, M.J., Tang, Q., 2014. The influence of future non-mitigated road transport emissions on regional ozone exceedences at global scale. Atmos. Environ. 89, 633–641.